

www.acsami.org Research Article

Remotely Controlled, Reversible, On-Demand Assembly and Reconfiguration of 3D Mesostructures via Liquid Crystal Elastomer Platforms

Yi Li, Chaoqian Luo, Kai Yu, and Xueju Wang*



Cite This: https://dx.doi.org/10.1021/acsami.0c21371



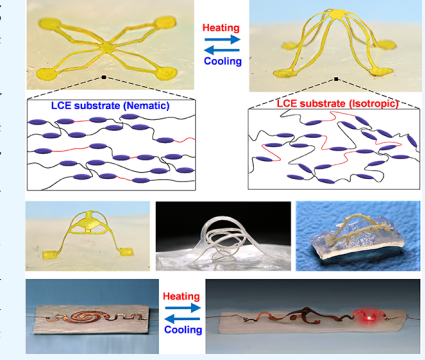
ACCESS

III Metrics & More



Supporting Information

ABSTRACT: Three-dimensional (3D) mesostructures are gaining rapidly growing interest due to their potential applications in a broad range of areas. Despite intensive studies, remotely controlled, reversible, on-demand assembly and reconfiguration of 3D mesostructures, which are desired for many applications, including robotics, minimally invasive biomedical devices, and deployable systems, remain a challenge. Here, we introduce a facile strategy to utilize liquid crystal elastomers (LCEs), a soft polymer capable of large, reversible shape changes, as a platform for reversible assembly and programming of 3D mesostructures via compressive buckling of two-dimensional (2D) precursors in a remote and on-demand fashion. The highly stretchable, reversible shapeswitching behavior of the LCE substrate, resulting from the soft elasticity of the material and the reversible nematic—isotropic transition of liquid crystal (LC) molecules upon remote thermal stimuli, provides deterministic thermal—mechanical control over the reversible assembly and reconfiguration processes. Demonstrations include experimental



results and finite element simulations of 3D mesostructures with diverse geometries and material compositions, showing the versatility and reliability of the approach. Furthermore, a reconfigurable light-emitting system is assembled and morphed between its "on" and "off" status via the LCE platform. These results provide many exciting opportunities for areas from remotely programmable 3D mesostructures to tunable electronic systems.

KEYWORDS: liquid crystal elastomers, reversible 3D assembly, mechanics-guided buckling, remote actuation, reconfigurable electronics

1. INTRODUCTION

Three-dimensional (3D) mesostructures are attracting increasing attention due to their potential applications in a wide range of fields, including micro-electromechanical systems (MEMS), ^{1–3} photonics, ^{4–6} biomedical devices, ^{7–9} soft robotics, ^{10–13} and metamaterials. ^{14–16} A number of techniques, including 3D printing, ^{1,4,17} self-assembly, ^{18–20} and controlled folding/rolling, ^{15,21,22} have been developed for the formation of 3D mesostructures of various materials and geometries. Recently, a mechanically guided 3D buckling technique is reported to provide a powerful means for deterministic transformation of planar precursors into 3D geometries of diverse material compositions and configurations at length scales from nano to macro. ^{19,23-25} In this technique, the release of a prestrained elastomer as an assembly platform exerts compressive forces to induce translational and rotational transformations of two-dimensional (2D) patterns into 3D configurations. Furthermore, manipulating the releasing time sequences of the elastomer platform allows the formation of morphable 3D mesostructures. 24-26 Despite intensive studies, most existing works based on this approach rely on mechanical stages to initiate the assembly process, which lacks the ability to achieve remotely triggered, on-demand assembly of structures and programmed shape reconfiguration. Such

limitation prevents potential applications of 3D structures in areas such as robotics and biomedical devices, where deployment and automated shape programming in enclosed or delicate environments are required.

Remote, on-demand actuation usually relies on the use of stimuli-responsive materials, including shape memory polymers, 19,27–29 liquid crystal elastomers (LCEs), 30–35 dielectric elastomers, 36–38 hydrogels, 39–43 magnetic composites, 12,44–46 and a combination of those materials. 47,48 Such materials can actively change their shapes under external stimuli such as heat, 19,27,49 light, 50,51 humidity, 41,52 and electric 37,53 and magnetic fields. 12,45,46 Recently, a bilayer of shape memory polymers and soft elastomers is utilized as an assembly platform to achieve the remotely triggered formation of 3D structures and aquatic systems via controlled mechanical buckling of 2D precursors. 27 The one-way shape change

Received: December 1, 2020 Accepted: February 3, 2021



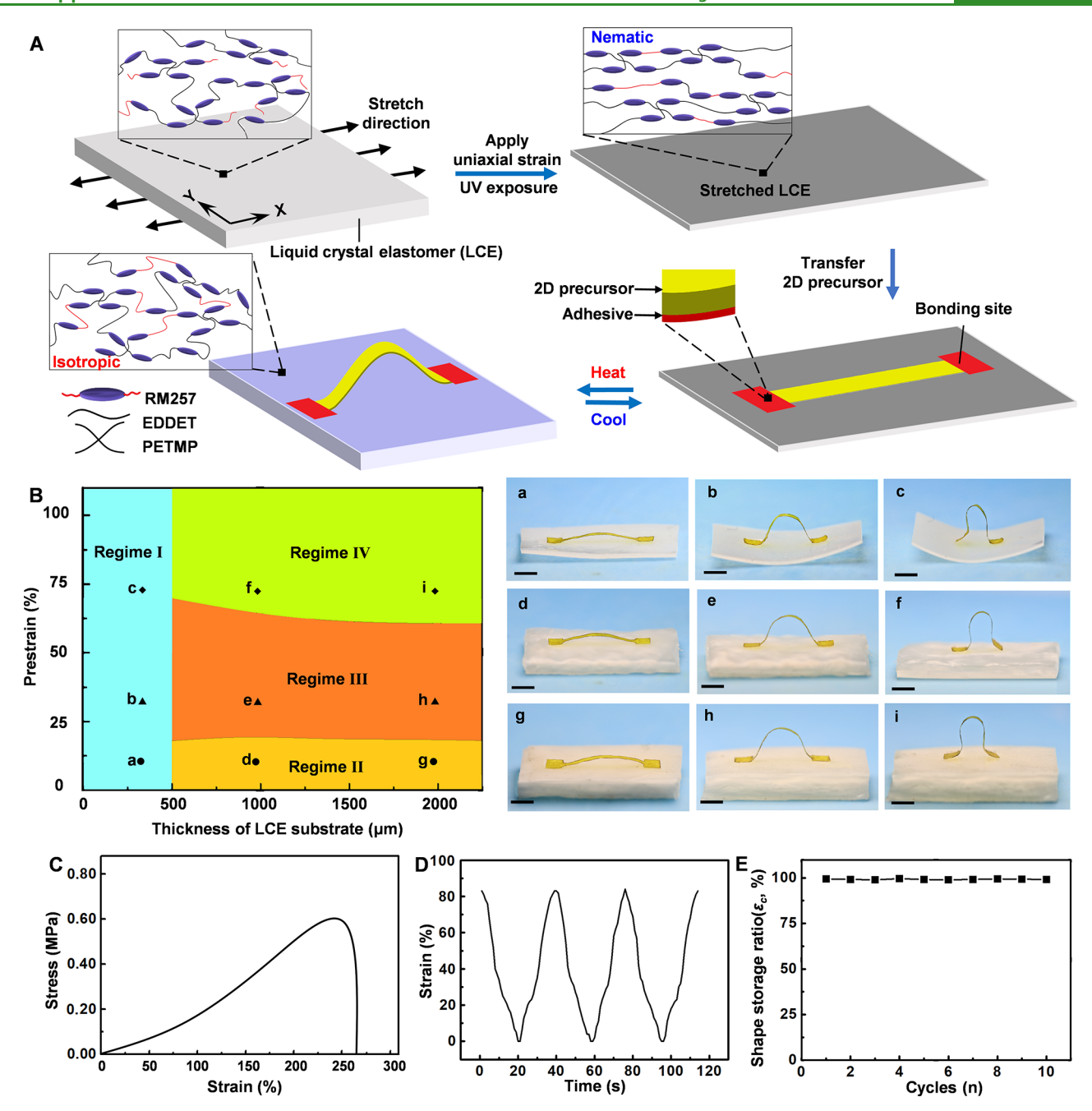


Figure 1. Reversible assembly and reconfiguration of 3D mesostructures via contraction—elongation deformations of a prestretched LCE substrate upon remote thermal stimuli. (A) Schematic illustration of the reversible assembly and shape reconfiguration processes for 3D structures. (B) Design phase diagram for the 3D assembly based on LCE platforms. Three-dimensional configurations corresponding to points (a—i) denoted in the diagram are shown. Scale bars, 2 mm. (C) Engineering stress—strain curve of LCEs. (D) Cyclic strain and recovery of the LCE upon heating and cooling across 62 °C via a heat gun. (E) Shape storage ratio of a ribbon structure over many assembly cycles based on LCE substrates.

behavior of SMPs, however, prevents further shape programming of the as-assembled 3D mesostructures. In addition, the need for integration with the elastomer into a bilayer for high stretchability complicates the processibility of the assembly platform.

In this work, we present a facile strategy for realizing remotely triggered, reversible 3D assembly and shape reconfiguration using liquid crystal elastomers (LCEs) as the assembly platform for mechanical buckling of 2D precursors. LCEs are a type of stimuli-responsive materials that are capable of large, reversible shape changes due to the combination of the soft elasticity of polymer networks and the self-organization

of liquid crystal (LC) phases. ^{30,31,50,54–65} The macroscopic shape-switching behaviors of LCEs are driven by the reversible nematic—isotropic transition of LC mesogens upon thermal stimuli. ^{50,54–56,66} Uniaxially stretched LCE substrates, which undergo reversible elongation—contraction deformations upon cyclic heating and cooling, are utilized to drive the compressive uniaxial buckling of 2D precursors into 3D mesostructures and subsequent shape reconfiguration. Three-dimensional structures of diverse material compositions and geometries and their reversible shape morphing behaviors are presented. The assembly of more complicated 3D configurations via biaxial buckling is also achieved by utilizing reconfigurable 3D LCE

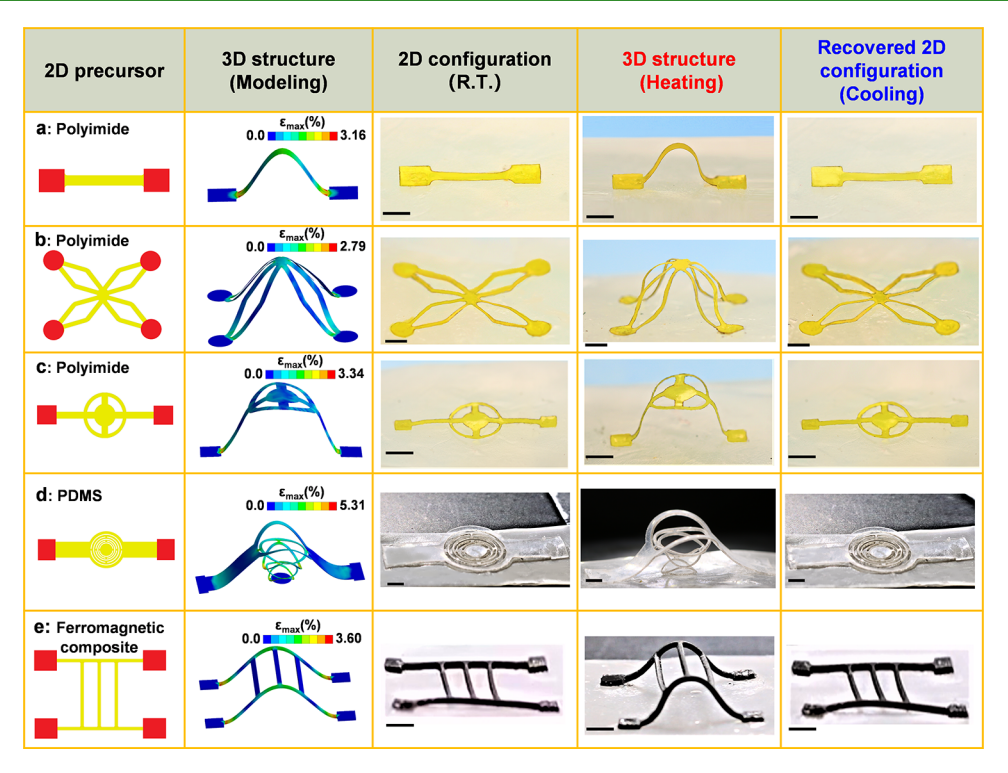


Figure 2. Experimental and finite element simulation results of 3D and 2D configurations over one reversible assembly/reconfiguration cycle. R.T. refers to room temperatre. Scale bars, 2 mm.

structures as the assembly platform. In addition, we present a reconfigurable light-emitting system via the reversible morphing of the LCE substrate responding to remote thermal stimuli. Such facile and versatile strategy for remotely controlled, reversible, and on-demand 3D assembly creates many opportunities for applications ranging from robotics to tunable 3D functional devices.

2. RESULTS AND DISCUSSION

2.1. Remotely Controlled, Reversible 3D Assembly and Reconfiguration via Uniaxially Stretched LCE Substrates. Figure 1A illustrates utilizing LCEs as a platform for remotely controlled, reversible assembly and reconfiguration of 3D mesostructures. The LCE used in this work is synthesized via a two-stage thiol-acrylate Michael addition reaction (TAMAP) methodology, 67,68 where mesogen 1,4-bis-[4-(3-acryloyloxypropyloxy)-benzoyloxy]-2-methylbenzene (RM257) is mixed with a crosslinker 2,2-(ethylenedioxy) diethanethiol (EDDET) and monomer pentaerythritol tetrakis (3-mercaptopropionate) (PETMP) to form an initial lightly crosslinked LCE polydomain network. To enable the subsequent photopolymerization capability, a photoinitiator (2-hydroxyethoxy)-2-methylpropiophenone (HHMP) is added to the solution (see details in the Materials and Methods section). Uniaxially stretching the lightly crosslinked LCE film (1.4 mm thick) induces elongation of the film and, therefore, mechanically aligns the LC molecules along the elongation direction (X-direction). The resulting ordered LC phases (nematic state) are permanently fixed under exposure to ultraviolet light (UV) (wavelength: 365-405 nm) via the second-stage photopolymerization reaction. Two-dimensional precursors consisting of thin-film materials are then transferred onto the stretched LCE substrate, with an ultrathin layer of superglue applied between the 2D precursor and the LCE

substrate at selective locations (bonding sites: strong interface) to form strong adhesion. The interfaces at all of the other regions (weak interface) are governed by relatively weak van der Waals forces.

Heating the LCE substrate above its isotropic clearing temperature (62 °C)⁶⁸ induces the transition from its nematic state into the isotropic state, which drives macroscopic contraction of the LCE into its original (nonstretched) shape. The mechanical contraction of the LCE substrate induces large compressive forces at bonding sites, which leads to in- and out-of-plane deformations of the 2D precursors into 3D configurations. Upon cooling to room temperature, the LCE substrate undergoes an isotropic-nematic transition, causing the elongation of the LCE and the geometrical transformation of the 3D buckled structure into its 2D configuration. It is worth noting that different prestrains of LCEs are required for buckling 3D structures of different geometries and materials. To achieve a well-controlled 3D assembly based on LCE substrates, we investigate the effects of key design parameters, including the thickness and the prestrain of LCEs, on the assembly of 3D mesostructures using a ribbon structure as an example. The LCE substrates of different thicknesses (200-2000 μ m) are used to buckle the 2D precursors of polyimide ribbons (9 μ m thick) under various prestrains (0-100%). As shown in Figure 1B, the configurations of the buckled structures can be divided into four regimes (I–IV). When the thickness of the LCE substrate is small (<500 μ m), the LCE substrate itself is deformed after the assembly process (points a, b, and c in Figure 1B) especially under a large prestrain, indicating that this range of LCEs is too thin for the 3D assembly of the ribbon structure. As the thickness of the LCE increases, the configurations of the assembled 3D structures can be grouped into three categories: (1) partial delamination (regime II), (2) full delamination of

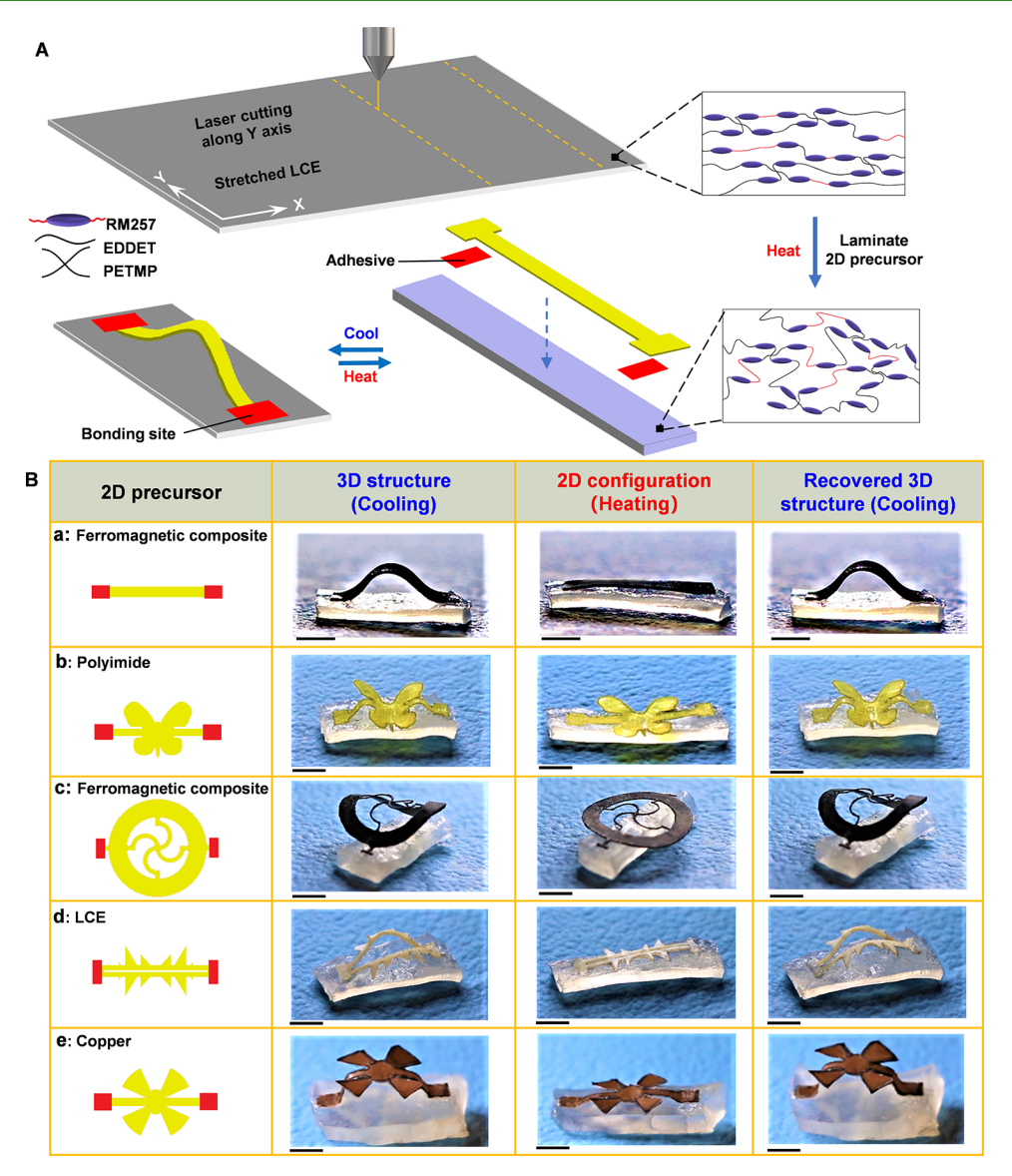


Figure 3. Formation of 3D mesostructures at room temperature via a prestretched LCE substrate. (A) Schematic illustration of the reversible assembly and shape reconfiguration process for a 3D structure driven by the elongation—contraction deformation of the LCE substrate in the direction perpendicular to the LC alignment. (B) Experimental results of 3D structures fabricated from various materials. Scale bars, 2 mm.

the weak interface (regime III), and (3) delamination of the strong interface (regime IV), similar to those reported for the typically used elastomer substrate for 3D assembly.⁶⁹ When the prestrain is small (regime II), releasing the prestrain in the LCE substrate causes partial delamination of the week interface (nonbonding site region) between the ribbon and the substrate (points d and g in Figure 1B). As the prestrain increases, the delamination propagates and induces full delamination of the weak interface but no delamination of the strong interface at the bonding sites (points e and h in Figure 1B), which represents the desired state for 3D assembly. Further increase in the prestrain leads to the delamination at the bonding sites and thereby undesired assembly (points f and i in Figure 1B). Such a design phase diagram provides important guidelines for the selection of LCE thicknesses and the appropriate prestrain for desired 3D assembly within regime III based on LCE platforms.

To evaluate the reliability of the reversible shape morphing behaviors of the LCE substrate, we further characterize the engineering stress—train curve of the LCE, as shown in Figure

1C. The maximum strain before the fracture is determined to be 256%, which is sufficiently large for the mechanically guided assembly of 3D structures via compressive buckling, where the prestrain is usually within 100%. Furthermore, the cyclic shape morphing behavior of LCEs is measured by recording the strain and recovery of the stretched LCE substrate along the direction of the LC molecular alignment (X-direction) while heating (via a heat gun at 90 °C) and cooling (via natural convection) across the isotropic clearing temperature (62 °C) for 10 cycles. Figure 1D shows the strain as a function of time for the first three shape-switching cycles, indicating highly consistent and repeatable elongation-contraction behaviors of the LCE substrate. In addition, to quantitatively investigate the repeatability of structure formation using the LCE substrate, we measure lateral dimensions of the buckled ribbon structure over 10 assembly cycles via the elongation-contraction deformation of the LCE substrate. Based on the measured dimensions, we further compute the shape storage ratio (ε_c) of the ribbon structure, which is defined below (Figure S1).

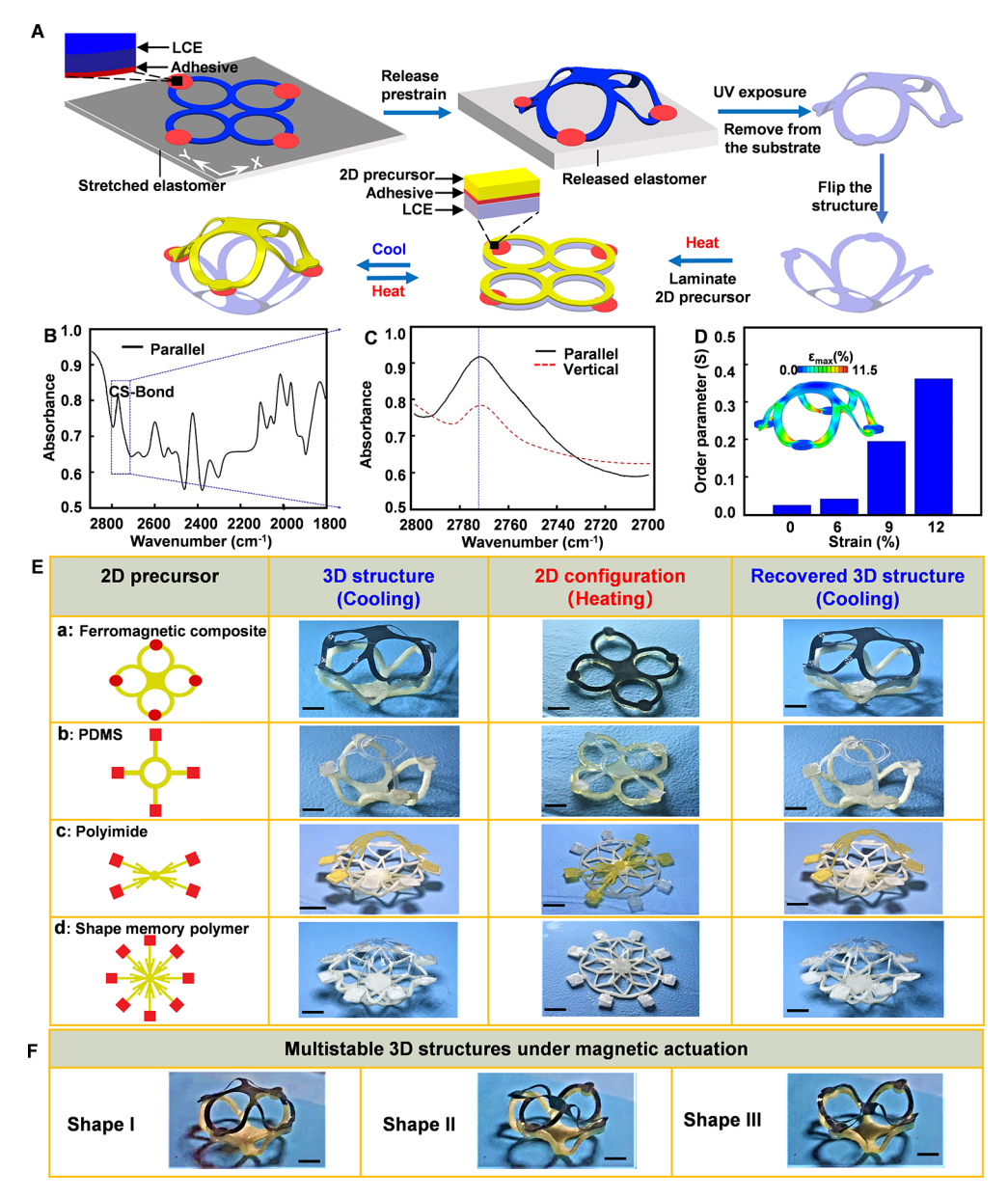


Figure 4. Reversible assembly and reconfiguration of diverse 3D mesostructures via the shape morphing of 3D LCE structure platforms. (A) Schematic illustration of the assembly and reversible shape reconfiguration process. (B) Polarized Fourier transform infrared spectroscopy (FTIR) trace of an LCE sample stretched by 12% engineering strain. The light polarization direction is parallel to the stretching direction. (C) Absorption peaks of the C–S bond when the polarization direction is, respectively, parallel and vertical to the stretching direction. (D) Order parameters of LCE at different amplitudes of tensile strain and the finite element analysis (FEA) modeling of the 3D LCE structure. (E) Diverse assembled 3D mesostructures and their reconfiguration upon heating and cooling the LCE structure. Scale bars, 2 mm. (F) Mutistable states of a 3D ferromagnetic PDMS composite structure under magnetic actuation. Scale bars, 2 mm.

$$\varepsilon_{c} = 1 - |L_{n} - L_{1}|/L_{1}, \quad n = 2 - 10$$
 (1)

where L_1 and L_n represent the distance between the two bonding sites of the ribbon structure after being buckled for the first and n^{th} time, respectively. As shown in Figure 1E, ε_c is determined to be above 99.4% for all of the tested cycles, which demonstrates the reliability of using LCEs as a platform for reversible assembly and reconfiguration of 3D mesostructures.

Figure 2 shows a collection of experimental results and finite element simulations of 3D structures formed from 2D precursors of polyimide (9 μ m thick), polydimethylsiloxane (PDMS) films (130 μ m thick), and ferromagnetic PDMS composites⁷¹ patterned using a CO₂ laser (VLS 3.50,

University Laser System, Norman, OK) (see details in the Materials and Methods section). Furthermore, the 3D buckled structures are shown to reversibly morph between their 2D and 3D configurations upon heating and cooling the LCE substrate across 62 °C using a heat gun. Such results show the immediate application of the approach to the reversible assembly and reconfiguration of diverse 3D structures of various materials. In addition, compared with the one-way assembly platform using a bilayer of SMP and elastomer, ²⁷ 3D assembly based on LCEs only requires a single layer of LCEs and can achieve reversible assembly and reconfiguration, providing a facile approach for remotely triggered, on-demand, reversible, and tunable 3D assembly. The processability of the LCE substrates using laser cutting and the compatibility of 2D

precursor fabrication with conventional planar techniques (photolithography and laser cutting) create a variety of design opportunities.

In addition to initiating the formation of 3D structures upon heating (above 62 °C) the LCE substrate, the reversible shape morphing of LCEs also allows initiating the assembly at room temperature (R.T.), serving as a complementary approach. Figure 3A schematically illustrates the assembly process. An LCE substrate (1.4 mm thick) is uniaxially stretched in the Xdirection, which leads to the mechanical alignment of mesogens along this direction. Subsequent photopolymerization fixes the stretched configuration. Laser cutting the LCE substrate forms the assembly platform. Upon heating, the ordered mesogens undergo a nematic-isotropic transition, causing the substrate to contract in the X-direction and to elongate in the Y-direction. A 2D pattern is then transferred onto the LCE substrate with bonding sites aligned along the Ydirection using an ultrathin layer of superglue between the 2D pattern and the LCE substrate. Cooling the LCE substrate to room temperature allows the mesogens to transition from its isotropic state into the nematic state, leading to the contraction of the LCE substrate in the Y-direction (perpendicular to the LC molecule alignment direction), thereby generating large compressive forces at bonding sites. Such forces induce translational and rotational deformations to geometrically transform the 2D pattern into a 3D shape. Heating the LCE substrate above 62 °C allows the LCE to transition from the nematic state into the isotropic state, morphing the 3D buckled structure into its 2D configuration.

Figure 3B and Movie S1 show a collection of reconfigurable 3D structures consisting of polymers including ferromagnetic PDMS composite (130 μ m thick), polyimide (9 μ m thick), LCE (200 μ m thick), and metals like copper (9 μ m thick), with geometries that resemble arcs, butterflies, bridges, and windmills. A thicker LCE substrate (1.9 mm thick), which provides larger actuation forces, is used for the formation and reconfiguration of the 3D copper structure (structure e). The diversity in constitutional materials and geometries demonstrates the wide applicability and versatility of this reversible assembly and reconfiguration strategy. In addition, compared to the initiation of 3D assembly at a high temperature (above 62 °C), 3D structures assembled using this strategy are formed at room temperature, which is easy to maintain and therefore advantageous for deployment environments where stable 3D structures are required under room temperature.

2.2. Three-Dimensional Assembly and Shape Reconfiguration via the Reversible Shape-Switching Behaviors of 3D LCE Structures. The reversible 3D assembly and shape reconfiguration strategy enabled by the uniaxially stretched LCE substrate introduced above allows uniaxial compressive buckling, due to the mechanical alignment of LCE molecules along the stretch direction. Previous studies show that biaxial compressive buckling can enable the assembly of more diverse 3D mesostructures. 19,23,26 To achieve remotely triggered, reversible assembly and reconfiguration of 3D mesostructures via biaxial buckling, we utilize a 3D LCE structure with spatially patterned LC molecules as an assembly platform. Figure 4A schematically illustrates the reversible 3D assembly and reconfiguration process, where 3D LCE structures fabricated via the compressive buckling of 2D LCE precursors (400 μ m thick) serve as the assembly platform. The LC molecular orientations in such 3D LCE structures undergo spatial patterning during the compressive

buckling process, which is permanently locked via the subsequent photopolymerization reaction. Heating the 3D LCE structure above 62 °C induces the transition from its nematic state into the isotropic state, driving the LCE structure to return to its 2D configuration. Target 2D precursors are then laminated onto the 2D LCE substrate with an ultrathin layer of superglue applied between the precursor and the LCE substrate at their overlapping bonding sites. Cooling the 2D LCE substrate to room temperature allows it to transition from the 2D configuration into the 3D shape due to the isotropicnematic transition, thereby inducing large compressive forces at bonding sites and leading to in- and out-of-plane deformations to transform the target 2D precursor into a 3D structure. Heating the 3D LCE structure above 62 °C allows it to recover its 2D state and therefore induces the target 3D structure to morph into the 2D configuration.

Due to the complicated strain distributions in 3D LCE structures, their LC orientations can be very complex. The alignment of mesogens and polymer chains in LCEs is usually characterized via wide-angle X-ray scattering (WAXS)⁷² and Fourier transform infrared spectroscopy (FTIR). 73 Both techniques, however, require 2D thin-film samples for testing, which prevents their applications to characterize the molecular alignment in 3D LCE structures. Since the mesogens and polymer chains tend to align in the direction of maximum principal strains, to explore the chain alignment in 3D LCE structures induced by compressive buckling, we perform FEA modeling on maximum principal strain distributions within the 3D structure (inset in Figure 4D) and then conduct polarized FTIR measurements of stretched LCE thin-film samples (450 μ m thick) with strain levels corresponding to those from FEA modeling. The functional groups on the chain backbone have the greatest light absorption when they are parallel to the polarizer and the weakest absorption when they are perpendicular. By comparing the height difference of absorption peaks in these two directions, the degree of alignment of various functional groups can be determined, which can be used to estimate the alignment degree of polymer chains. Polarized FTIR tests are first performed on LCE samples stretched by 12% engineering strain, which is close to the maximum principal strain within the deformed structure as revealed in the FEA results, using a Nicolet 6700 FTIR spectrometer (Thermo Scientific, Waltham, MA). The FTIR traces are collected in both the parallel direction and the vertical direction of stretch. The absorption of C-S groups, which are on the backbone of polymer chains, is used to evaluate the chain alignment degree. Since the alignment of the polymer chains and the mesogen units are inherently linked, this peak is used to characterize the overall sample alignment. However, since the C-S bonds are not on the mesogen, the alignment degree of the mesogen cores may be higher.

The FTIR trace of the LCE sample in the parallel direction of stretch is shown in Figure 4B, where the absorption peak at ~2770 cm⁻¹ is identified as the C–S peak. Please note that C–S bonds typically have an absorption peak at 710–570 cm⁻¹. Since the FTIR sample is relatively thick, a peak is not detected in this region. On the other hand, the thiol S–H bond, which is located at the tail of the spacer EDDET and PETMP, has an absorption peak around 2770 cm⁻¹. During the LCE synthesis, the S–H bonds are fully consumed and transformed to C–S bonds after the thiol-ene reaction. However, a small peak is still observed at the same wavenumber. Similar observations are reported previously, ^{68,75} wherein the LCEs

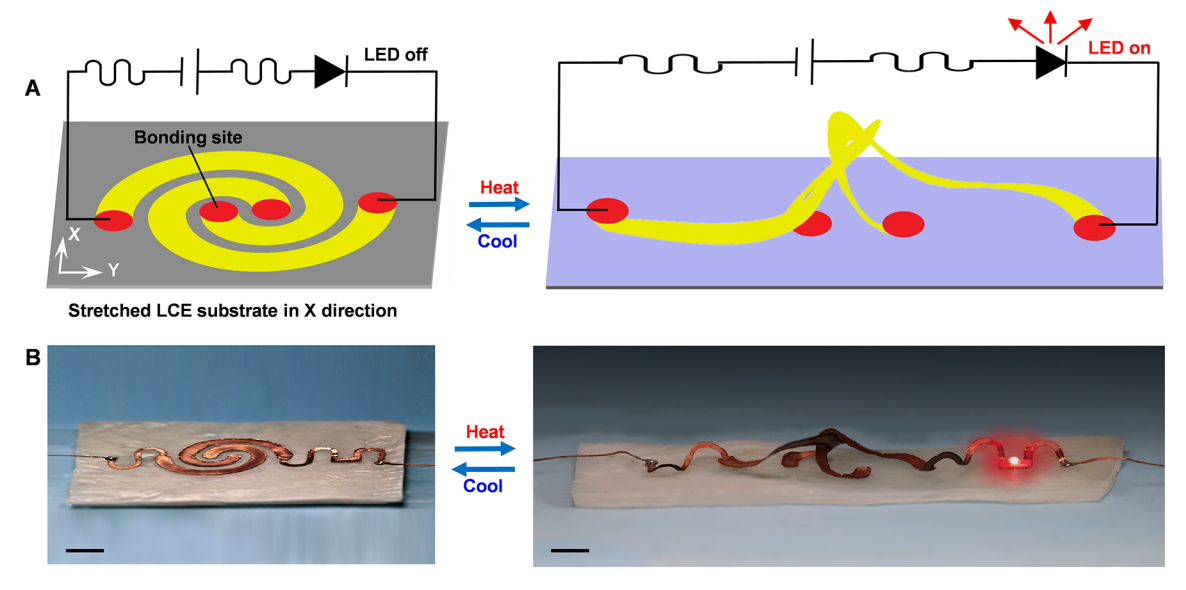


Figure 5. Reconfigurable light-emitting system. (A) Schematic illustration of the assembly and reconfiguration of a light-emitting system via the LCE platform. (B) Experimental results of the 2D (LED off) and 3D configurations (LED on) of the light-emitting system under cooling and heating of the LCE substrate. Scale bars, 3 mm.

are synthesized using the same chemistry. This suggests that in addition to an absorption peak at 710–570 cm⁻¹, the newly formed C–S bond can still absorb energy at 2770 cm⁻¹. As seen from Figure 4C, the C–S group has a greater absorption peak when parallel to the polarizer and a weaker peak when perpendicular. The alignment degree of C–S groups is quantified using a scalar order parameter, S. The peak height of the C–S group at different polarizations is used to calculate the dichroic ratio, D, which is determined as⁷³

$$D = \frac{H_{\text{max}}}{H_{\text{min}}} \tag{2}$$

where $H_{\rm max}$ is the maximum absorbance in the parallel direction and $H_{\rm min}$ is the minimum absorbance in the vertical direction. The order parameter S is determined as 73

$$S = \frac{D-1}{D+2} \tag{3}$$

Here, S=0 means no alignment and the chains are randomly distributed; S=1 means perfect alignment of polymer chains. The measured order parameters at different strain levels are shown in Figure 4D. It is observed that the order parameter increases with the strain level, with S values determined to be 0.195 and 0.377 for strains of 9% and 12%, respectively, suggesting a notable alignment of polymer chains within the LCE sample. Please note that during the shape changes, the actuation strain increases with the order parameter of polymer chains.

Figure 4E presents representative 3D structures that are assembled from ferromagnetic PDMS composite (130 μ m thick), pure PDMS (130 μ m thick), polyimide (50 μ m thick), and shape memory polymer (SMP, 70 μ m thick) thin films via the shape morphing of 3D LCE structures (see details in the Materials and Methods section). It is worth noting that the magnitude and the nature of the strain induced by the 3D–2D shape morphing of the LCE platform provide deterministic control over the assembly and reconfiguration processes. The same LCE assembly platform can be used to form various target 3D mesostructures (structures a and b in Figure 4E). In

addition, the number and the size of the bonding sites of the 2D precursors can be different from those of the underlying LCE substrate (structure c and d in Figure 4E), which allows more flexibility for the assembly of a diversity of 3D mesostructures. Interestingly, the buckled 3D mesostructure can be further reconfigured into multiple stable states via additional external stimuli. For example, Figure 4F presents three stable configurations of the 3D ferromagnetic PMDS composite structure (structure a in Figure 4E) under magnetic actuation applied via a portable magnet (D8Y0, K&J magnetics). While this work focuses on the reversible and remotely triggered assembly of 3D structures enabled by LCE platforms, the results in Figure 4F suggest that multistable and multistimuli responsive composite structures could be of great interest in applications such as soft robotics and deserves our future study.

2.3. Remotely Controlled, Reconfigurable Light-Emitting System. The reversible shape morphing and soft elasticity properties of LCEs enable the use of LCEs as a powerful platform for remotely triggered, reversible assembly and reconfiguration of 3D mesostructures. In addition, such characteristics are also desired for a lot of applications such as in soft robotics and tunable electronic devices. As an example, we assemble a reconfigurable light-emitting system driven by the elongation-contraction behavior of the LCE substrate under heating and cooling. Figure 5A schematically illustrates the design principle, where a 2D precursor of copper (9 μ m thick) in spiral geometries is connected to a light-emitting diode (LED) and laminated onto a prestreched LCE substrate (1.4 mm thick) that is uniaxially stretched in the X-direction. Heating above 62 °C causes the LCE substrate to contract in the X-direction and to elongate in the Y-direction, buckling the 2D copper precursor into a 3D structure. Upon 3D assembly, the copper ribbons are brought into contact and thereby form a closed circuit to turn the LED on. Cooling the LCE substrate to room temperature leads to the contraction of the LCE substrate in the Y-direction and recovers the 3D structure to its 2D state, where the copper ribbons are separated, turning the LED off. Figure 5B shows experimental results of the reconfigurable light-emitting system upon heating and cooling the LCE substrate using a heat gun. Such a remotely tunable electronic system demonstrates the capability of the LCE platform for the on-demand, reversible shape morphing of 3D functional devices.

3. CONCLUSIONS

To sum up, this work introduces facile strategies for remotely controlled, reversible assembly and programming of 3D mesostructures via the highly stretchable, shape-switching behavior of LCE substrates. Integrated FEA modeling and experiments of diverse 3D mesostructures assembled from various materials (polymers, metals, and composites) and their reversible shape reconfiguration illustrate the versatility of the approach. Furthermore, the processibility of LCEs and the compatibility of the approach with conventional planar techniques (laser cutting, molding, and photolithography) present a variety of design opportunities. The fabricated lightemitting system shows reversible 2D and 3D reconfiguration under remote thermal stimuli to achieve the control of the "on" and "off" status of the LED, creating many opportunities for applications in tunable 3D functional devices and many others. In addition, the developed strategy for reversible 3D assembly and shape reconfiguration also provides important insights for the design of other programmable 3D structures and systems including origami/kirigami and deployable devices.

4. MATERIALS AND METHODS

- 4.1. Synthesis of LCE Films. In this study, the two-stage thiolacrylate Michael addition-photopolymerization (TAMAP) reaction was used to synthesize the liquid crystal elastomer (LCE). ^{67,68} 1,4-Bis-[4-(3-acryloyloxypropyloxy)-benzoyloxy]-2-methylbenzene (RM257) was purchased from Wilshire Technologies and used as received without further purification. 2,2-(Ethylenedioxy) diethanethiol (EDDET, a di-thiol monomer), pentaerythritol tetrakis(3mercaptopropionate) (PETMP, a tetrafunctional thiol crosslinking monomer), (2-hydroxyethoxy)-2-methylpropiophenone (HHMP, a photoinitiator), dipropylamine (DPA), and toluene were purchased from Sigma Aldrich and used as received. Forty weight percent (40 wt %) of toluene was added to the RM257 powder, and the mixture was heated to 62 °C to dissolve RM257. After the solution was cooled to room temperature, PETMP and EDDET were added with a molar ratio of 85:15. This is followed by dissolving 0.38 wt % of HHMP into the solution to enable the second-stage photopolymerization reaction. One mole percent (1 mol%) of diluted DPA in toluene was then mixed into the solution using a planetary mixer (AR-100, Thinky) at 2000 rpm for 30 s, followed by deforming air bubbles for 30 s. The solution was immediately coated onto a high-density polyethylene (HDPE) mold to form LCE films. After curing at room temperature for 12 h, LCE gel samples were obtained, which were then placed in a vacuum oven at 80 °C for 12 h to evaporate the toluene.
- 4.2. Remotely Triggered, Reversible 3D Assembly and Shape Reconfiguration via Uniaxially Stretched LCE Substrates. The formed LCE film substrate (thickness: 1.4 mm) was uniaxially stretched via a mechanically controlled stretcher, followed by exposure to ultraviolet light (UV; wavelength: 365–400 nm) for 3–4 min to fix the stretched configuration. Two-dimensional precursors patterned with a CO₂ laser (VLS 3.50, University Laser System, Norman, OK) were transferred onto the permanently stretched LCE substrate. An ultrathin layer of superglue was applied between the 2D precursor and the LCE substrate above 62 °C induced the contraction of the elongated shape into its original configuration and initiated compressive buckling of the 2D precursor into a 3D structure. After cooling to room temperature, the LCE substrate elongated, leading to the recovery of the 3D buckled structure to its 2D configuration.

To enable the initiation of 3D assembly at room temperature, the LCE substrate was first uniaxially stretched (strain: ε_{κ}) using a mechanically controlled stretcher. Due to the Poisson effect of LCEs (Poisson's ratio: v = 0.45), such elongation caused contraction ($\varepsilon_v =$ $-v\varepsilon_r$) in the direction (Y-direction) perpendicular to the stretched direction (X-direction). The stretched LCE substrate was exposed to ultraviolet light (UV; wavelength: 365-405 nm) for 3-4 min and was then patterned into a rectangle shape as the assembly platform using a CO2 laser. Upon heating, the LCE substrate elongated in the Ydirection. Two-dimensional patterns were then laminated onto the LCE substrate with the application of a thin layer of superglue at the bonding sites. Upon cooling to room temperature, the LCE substrate contracted in the Y-direction and compressively buckled the 2D pattern into a 3D structure. Upon further heating above 62 °C, the LCE substrate elongated and morphed the 3D structure into its 2D configuration.

- 4.3. Synthesis of Ferromagnetic PDMS Composite Films. NdFeB microparticles (average diameter: 5 μ m; MQFP-B-2007609—089, Magnequench) were mixed with PDMS resin (Sylgard 184, Dow Corning) at a volume ratio of 1:5. A planetary mixer (AR-100, Thinky) was used for rigorous mixing (2000 rpm for 2 min), which was followed by defoaming the solution at 2000 rpm for 1 min to remove air bubbles. The mixture was then spin-coated onto a planar glass substrate at 500 rpm for 15 s and cured at room temperature to form thin films (130 μ m thick).
- **4.4. Synthesis of SMP films.** Styrene (ST), butyl acrylate (BA), poly(ethylene glycol) diacrylate (PEGDA, $M_{\rm n}=575$), and benzoyl peroxide (BPO) were all purchased from Sigma Aldrich and used as received. ST (1.21 g), BA (0.8 g), and PEGDA (0.1 g) were weighed into a bottle and mixed using a planetary mixer (AR-100, Thinky) at 2000 rpm for 1 min, followed by deforming air bubbles for 30 s. BPO (0.02 g) was weighed and dissolved into the mixture, which was then poured into a sealed glass mold and transferred into an oven at 80 °C for curing for 2 h to complete the synthesis. Demolding was conducted in water to release the SMP films (70 μ m thick).
- 4.5. Remotely Triggered, Reversible 3D Assembly via the Shape Morphing of 3D LCE Structures. A 3D LCE structure (400 um thick) was first fabricated following the previously reported compressive buckling technique.²³ The buckled 3D LCE structure was exposed to ultraviolet light (UV; wavelength: 365-405 nm) for 3-4 min to fix the 3D shape, which was then released from the substrate to become freestanding by dissolving a water-soluble tape at the bonding sites. Upon heating, the freestanding 3D LCE structure was reconfigured into its 2D state, serving as an assembly platform. Target 2D precursors were transferred onto the 2D LCE substrate with an ultrathin layer of superglue applied at the bonding sites. Upon cooling, the 2D LCE substrate morphed into its 3D configuration, thereby geometrically transforming the target 2D precursors into 3D structures. Upon heating above 62 °C, the 3D LCE structure recovered its 2D state and transformed the buckled 3D structures into their 2D configurations.
- **4.6. Polarized FTIR Analysis of LC Alignment.** Polarized FTIR tests were performed in the transmission mode at room temperature on a Nicolet 6700 FTIR spectrometer (Thermo Scientific, Waltham, MA) with a KRS-5 wire grid polarizer and a custom-built sample holder. The LCE sample with a dimension of 16.5 mm × 3.9 mm × 0.45 mm was stretched by 12% engineering strain, which is the maximum principal strain within the deformed structure as revealed in the FEA results. The FTIR traces were collected both in the parallel direction and the vertical direction of stretch. The strain of the LCE samples during the FTIR measurements was changed from 0 to 12%, and the abovementioned tests and calculations were repeated.
- **4.7.** Assembly of the Light-Emitting System. An LCE film (1.4 mm thick) was first uniaxially stretched in the X-direction and exposed to ultraviolet light (UV; wavelength: 365-405 nm) for 3-4 min to serve as the assembly platform. Thin copper films (9 μ m thick) were patterned into spiral geometries using a CO₂ laser, which were then laminated onto the LCE substrate with the application of a thin layer of superglue at the bonding sites. An LED was integrated into the structures, and a power of 3 V was supplied to the circuit. Upon

heating above 62 $^{\circ}$ C, the LCE substrate elongated in the Y-direction and buckled the 2D pattern into a 3D structure to enable two copper ribbons to contact each other, turning the LED on. When it cooled to room temperature, the LCE substrate contracted and morphed the 3D structure into its 2D configuration to separate the two copper ribbons, thereby turning the LED off.

4.8. Finite Element Modeling. Finite element analysis (FEA) was carried out using the commercial software ANSYS. Four-node shell elements were used for the simulation of compressive buckling of 2D precursors. To ensure computational accuracy, refined meshes were adopted. The following elastic moduli (E) and Poisson's ratios (ν) were used for the simulation of LCEs, PDMS, and magnetic PDMS composite: $E_{\rm LCE} = 0.126$ MPa, $v_{\rm LCE} = 0.45$; $E_{\rm PDMS} = 1.3$ MPa, $v_{\rm PDMS} = 0.40$; and $E_{\rm PDMS} = 1.4$ Mpa, $E_{\rm PDMS} = 0.40$.

ASSOCIATED CONTENT

Supporting Information

The Supporting Information is available free of charge at https://pubs.acs.org/doi/10.1021/acsami.0c21371.

Schematic illustration of the dimensions of the ribbon structure over multiple assembly cycles (Figure S1) (PDF)

Reversible assembly and reconfiguration processes of 3D structures via the shape morphing of an LCE substrate under remote heating and cooling (Movie S1) (MP4)

AUTHOR INFORMATION

Corresponding Author

Xueju Wang — Department of Materials Science and Engineering, University of Connecticut, Storrs, Connecticut 06269, United States; orcid.org/0000-0002-0669-8759; Email: xueju.wang@uconn.edu

Authors

Yi Li — Department of Materials Science and Engineering, University of Connecticut, Storrs, Connecticut 06269, United

Chaoqian Luo – Department of Mechanical Engineering, University of Colorado Denver, Denver, Colorado 80217, United States

Kai Yu — Department of Mechanical Engineering, University of Colorado Denver, Denver, Colorado 80217, United States; orcid.org/0000-0001-9067-1673

Complete contact information is available at: https://pubs.acs.org/10.1021/acsami.0c21371

Author Contributions

The manuscript was written through the contributions of all authors. All authors have given approval to the final version of the manuscript.

Notes

The authors declare no competing financial interest.

ACKNOWLEDGMENTS

The authors acknowledge the support from NSF CMMI #2103012 and the Institute of Materials Science at the University of Connecticut.

REFERENCES

(1) Wu, S.-Y.; Yang, C.; Hsu, W.; Lin, L. 3D-printed microelectronics for integrated circuitry and passive wireless sensors. *Microsyst. Nanoeng.* **2015**, *1*, No. 15013.

I

- (2) Cui, J.; Huang, T.-Y.; Luo, Z.; Testa, P.; Gu, H.; Chen, X.-Z.; Nelson, B. J.; Heyderman, L. J. Nanomagnetic encoding of shape-morphing micromachines. *Nature* **2019**, *575*, 164–168.
- (3) Miskin, M. Z.; Dorsey, K. J.; Bircan, B.; Han, Y.; Muller, D. A.; McEuen, P. L.; Cohen, I. Graphene-based bimorphs for micron-sized, autonomous origami machines. *Proc. Natl. Acad. Sci. U.S.A.* **2018**, *115*, 466
- (4) Huang, X.; Guo, Q.; Yang, D.; Xiao, X.; Liu, X.; Xia, Z.; Fan, F.; Qiu, J.; Dong, G. Reversible 3D laser printing of perovskite quantum dots inside a transparent medium. *Nat. Photonics* **2020**, *14*, 82–88.
- (5) Liu, Y.; Wang, H.; Ho, J.; Ng, R. C.; Ng, R. J. H.; Hall-Chen, V. H.; Koay, E. H. H.; Dong, Z.; Liu, H.; Qiu, C.-W.; Greer, J. R.; Yang, J. K. W. Structural color three-dimensional printing by shrinking photonic crystals. *Nat. Commun.* **2019**, *10*, No. 4340.
- (6) Klatt, M. A.; Steinhardt, P. J.; Torquato, S. Phoamtonic designs yield sizeable 3D photonic band gaps. *Proc. Natl. Acad. Sci. U.S.A.* **2019**, *116*, 23480.
- (7) Urciuolo, A.; Poli, I.; Brandolino, L.; Raffa, P.; Scattolini, V.; Laterza, C.; Giobbe, G. G.; Zambaiti, E.; Selmin, G.; Magnussen, M.; Brigo, L.; De Coppi, P.; Salmaso, S.; Giomo, M.; Elvassore, N. Intravital three-dimensional bioprinting. *Nat. Biomed. Eng.* **2020**, *4*, 901–915.
- (8) Li, J.; Li, R.; Du, H.; Zhong, Y.; Chen, Y.; Nan, K.; Won, S. M.; Zhang, J.; Huang, Y.; Rogers, J. A. Ultrathin, Transferred Layers of Metal Silicide as Faradaic Electrical Interfaces and Biofluid Barriers for Flexible Bioelectronic Implants. ACS Nano 2019, 13, 660–670.
- (9) Derakhshanfar, S.; Mbeleck, R.; Xu, K.; Zhang, X.; Zhong, W.; Xing, M. 3D bioprinting for biomedical devices and tissue engineering: A review of recent trends and advances. *Bioact. Mater.* **2018**, 3, 144–156.
- (10) Hu, W.; Lum, G. Z.; Mastrangeli, M.; Sitti, M. Small-scale soft-bodied robot with multimodal locomotion. *Nature* **2018**, *554*, 81–85.
- (11) Liu, J. A.-C.; Gillen, J. H.; Mishra, S. R.; Evans, B. A.; Tracy, J. B. Photothermally and magnetically controlled reconfiguration of polymer composites for soft robotics. *Science Adv.* **2019**, *S*, No. eaaw2897.
- (12) Kim, Y.; Parada, G. A.; Liu, S. D.; Zhao, X. H. Ferromagnetic soft continuum robots. Sci. Rob. 2019, 4, No. eaax7329.
- (13) Xu, W.; Gracias, D. H. Soft Three-Dimensional Robots with Hard Two-Dimensional Materials. ACS Nano 2019, 13, 4883–4892.
- (14) Neville, R. M.; Scarpa, F.; Pirrera, A. Shape morphing Kirigami mechanical metamaterials. *Sci. Rep.* **2016**, *6*, No. 31067.
- (15) Silverberg, J. L.; Evans, A. A.; McLeod, L.; Hayward, R. C.; Hull, T.; Santangelo, C. D.; Cohen, I. Using origami design principles to fold reprogrammable mechanical metamaterials. *Science* **2014**, *345*, 647–650.
- (16) Tang, Y.; Li, Y.; Hong, Y.; Yang, S.; Yin, J. Programmable active kirigami metasheets with more freedom of actuation. *Proc. Natl. Acad. Sci. U.S.A.* **2019**, *116*, 26407–26413.
- (17) Zhang, Y.; Dong, Z.; Li, C.; Du, H.; Fang, N. X.; Wu, L.; Song, Y. Continuous 3D printing from one single droplet. *Nat. Commun.* **2020**, *11*, No. 4685.
- (18) Abdullah, A. M.; Li, X.; Braun, P. V.; Rogers, J. A.; Hsia, K. J. Kirigami-Inspired Self-Assembly of 3D Structures. *Adv. Funct. Mater.* **2020**, *30*, No. 1909888.
- (19) Wang, X.; Guo, X.; Ye, J.; Zheng, N.; Kohli, P.; Choi, D.; Zhang, Y.; Xie, Z.; Zhang, Q.; Luan, H.; Nan, K.; Kim, B. H.; Xu, Y.; Shan, X.; Bai, W.; Sun, R.; Wang, Z.; Jang, H.; Zhang, F.; Ma, Y.; Xu, Z.; Feng, X.; Xie, T.; Huang, Y.; Zhang, Y.; Rogers, J. A. Freestanding 3D Mesostructures, Functional Devices, and Shape-Programmable Systems Based on Mechanically Induced Assembly with Shape Memory Polymers. *Adv. Mater.* 2019, 31, No. 1805615.
- (20) Xu, W.; Ledin, P. A.; Shevchenko, V. V.; Tsukruk, V. V. Architecture, Assembly, and Emerging Applications of Branched Functional Polyelectrolytes and Poly(ionic liquid)s. *ACS Appl. Mater. Interfaces* **2015**, *7*, 12570–12596.
- (21) Xia, Y.; Cedillo-Servin, G.; Kamien, R. D.; Yang, S. Guided Folding of Nematic Liquid Crystal Elastomer Sheets into 3D via Patterned 1D Microchannels. *Adv. Mater.* **2016**, 28, 9637–9643.

- (22) Sundaram, S.; Kim, D. S.; Baldo, M. A.; Hayward, R. C.; Matusik, W. 3D-Printed Self-Folding Electronics. *ACS Appl. Mater. Interfaces* **2017**, *9*, 32290–32298.
- (23) Xu, S.; Yan, Z.; Jang, K.-I.; Huang, W.; Fu, H.; Kim, J.; Wei, Z.; Flavin, M.; McCracken, J.; Wang, R.; Badea, A.; Liu, Y.; Xiao, D.; Zhou, G.; Lee, J.; Chung, H. U.; Cheng, H.; Ren, W.; Banks, A.; Li, X.; Paik, U.; Nuzzo, R. G.; Huang, Y.; Zhang, Y.; Rogers, J. A. Assembly of micro/nanomaterials into complex, three-dimensional architectures by compressive buckling. *Science* 2015, 347, 154.
- (24) Zhao, H.; Li, K.; Han, M.; Zhu, F.; Vazquez-Guardado, A.; Guo, P.; Xie, Z.; Park, Y.; Chen, L.; Wang, X.; Luan, H.; Yang, Y.; Wang, H.; Liang, C.; Xue, Y.; Schaller, R. D.; Chanda, D.; Huang, Y.; Zhang, Y.; Rogers, J. A. Buckling and twisting of advanced materials into morphable 3D mesostructures. *Proc. Natl. Acad. Sci. U.S.A.* **2019**, *116*, 13239–13248.
- (25) Liu, Y.; Wang, X.; Xu, Y.; Xue, Z.; Zhang, Y.; Ning, X.; Cheng, X.; Xue, Y.; Lu, D.; Zhang, Q.; Zhang, F.; Liu, J.; Guo, X.; Hwang, K.-C.; Huang, Y.; Rogers, J. A.; Zhang, Y. Harnessing the interface mechanics of hard films and soft substrates for 3D assembly by controlled buckling. *Proc. Natl. Acad. Sci. U.S.A.* **2019**, *116*, 15368.
- (26) Fu, H. R.; Nan, K. W.; Bai, W. B.; Huang, W.; Bai, K.; Lu, L. Y.; Zhou, C. Q.; Liu, Y. P.; Liu, F.; Wang, J. T.; Han, M. D.; Yan, Z.; Luan, H. W.; Zhang, Y. J.; Zhang, Y. T.; Zhao, J. N.; Cheng, X.; Li, M. Y.; Lee, J. W.; Liu, Y.; Fang, D. N.; Li, X. L.; Huang, Y. G.; Zhang, Y. H.; Rogers, J. A. Morphable 3D mesostructures and microelectronic devices by multistable buckling mechanics. *Nat. Mater.* **2018**, *17*, 268–276
- (27) Park, J. K.; Nan, K.; Luan, H.; Zheng, N.; Zhao, S.; Zhang, H.; Cheng, X.; Wang, H.; Li, K.; Xie, T.; Huang, Y.; Zhang, Y.; Kim, S.; Rogers, J. A. Remotely Triggered Assembly of 3D Mesostructures Through Shape-Memory Effects. *Adv. Mater.* **2019**, *31*, No. e1905715.
- (28) Zarek, M.; Layani, M.; Cooperstein, I.; Sachyani, E.; Cohn, D.; Magdassi, S. 3D Printing of Shape Memory Polymers for Flexible Electronic Devices. *Adv. Mater.* **2016**, *28*, 4449–4454.
- (29) Lei, M.; Yu, K.; Lu, H.; Qi, H. J. Influence of structural relaxation on thermomechanical and shape memory performances of amorphous polymers. *Polymer* **2017**, *109*, 216–228.
- (30) Maeng, J.; Rihani, R. T.; Javed, M.; Rajput, J. S.; Kim, H.; Bouton, I. G.; Criss, T. A.; Pancrazio, J. J.; Black, B. J.; Ware, T. H. Liquid crystal elastomers as substrates for 3D, robust, implantable electronics. *J. Mater. Chem. B* **2020**, *8*, 6286–6295.
- (31) Shahsavan, H.; Aghakhani, A.; Zeng, H.; Guo, Y.; Davidson, Z. S.; Priimagi, A.; Sitti, M. Bioinspired underwater locomotion of light-driven liquid crystal gels. *Proc. Natl. Acad. Sci. U.S.A.* **2020**, *117*, 5125–5133.
- (32) Gantenbein, S.; Masania, K.; Woigk, W.; Sesseg, J. P. W.; Tervoort, T. A.; Studart, A. R. Three-dimensional printing of hierarchical liquid-crystal-polymer structures. *Nature* **2018**, *561*, 226–230.
- (33) Barnes, M.; Verduzco, R. Direct shape programming of liquid crystal elastomers. *Soft Matter* **2019**, *15*, 870–879.
- (34) Barnes, M.; Sajadi, S.; Parekh, S.; Rahman, M. M.; Ajayan, P. M.; Verduzco, R. Reactive 3D Printing of Shape Programmable Liquid Crystal Elastomer Actuators. *ACS Appl. Mater. Interfaces* **2020**, *12*, 28692–28699.
- (35) Wang, Z.; Wang, Z.; Zheng, Y.; He, Q.; Wang, Y.; Cai, S. Three-dimensional printing of functionally graded liquid crystal elastomer. *Sci. Adv.* **2020**, *6*, No. eabc0034.
- (36) Chortos, A.; Hajiesmaili, E.; Morales, J.; Clarke, D. R.; Lewis, J. A. 3D Printing of Interdigitated Dielectric Elastomer Actuators. *Adv. Funct. Mater.* **2020**, *30*, No. 1907375.
- (37) Hajiesmaili, E.; Clarke, D. R. Reconfigurable shape-morphing dielectric elastomers using spatially varying electric fields. *Nat. Commun.* **2019**, *10*, No. 183.
- (38) Goh, Y. F.; Akbari, S.; Khanh Vo, T. V.; Koh, S. J. A. Electrically-Induced Actuation of Acrylic-Based Dielectric Elastomers in Excess of 500% Strain. *Soft Rob.* **2018**, *5*, 675–684.

- (39) Qin, H.; Zhang, T.; Li, N.; Cong, H.-P.; Yu, S.-H. Anisotropic and self-healing hydrogels with multi-responsive actuating capability. *Nat. Commun.* **2019**, *10*, No. 2202.
- (40) Yuk, H.; Lin, S.; Ma, C.; Takaffoli, M.; Fang, N. X.; Zhao, X. Hydraulic hydrogel actuators and robots optically and sonically camouflaged in water. *Nat. Commun.* **2017**, *8*, No. 14230.
- (41) Ionov, L. Biomimetic Hydrogel-Based Actuating Systems. *Adv. Funct. Mater.* **2013**, 23, 4555–4570.
- (42) Gladman, A. S.; Matsumoto, E. A.; Nuzzo, R. G.; Mahadevan, L.; Lewis, J. A. Biomimetic 4D printing. *Nat. Mater.* **2016**, *15*, 413–418
- (43) Yu, C.; Duan, Z.; Yuan, P.; Li, Y.; Su, Y.; Zhang, X.; Pan, Y.; Dai, L. L.; Nuzzo, R. G.; Huang, Y. Electronically Programmable, Reversible Shape Change in Two-and Three-Dimensional Hydrogel Structures. *Adv. Mater.* **2013**, *25*, 1541–1546.
- (44) Yen, T. J.; Padilla, W. J.; Fang, N.; Vier, D. C.; Smith, D. R.; Pendry, J. B.; Basov, D. N.; Zhang, X. Terahertz Magnetic Response from Artificial Materials. *Science* **2004**, *303*, 1494–1496.
- (45) Kwok, S. W.; Morin, S. A.; Mosadegh, B.; So, J. H.; Shepherd, R. F.; Martinez, R. V.; Smith, B.; Simeone, F. C.; Stokes, A. A.; Whitesides, G. M. Magnetic Assembly of Soft Robots with Hard Components. *Adv. Funct. Mater.* **2014**, 24, 2180–2187.
- (46) Lum, G. Z.; Ye, Z.; Dong, X.; Marvi, H.; Erin, O.; Hu, W.; Sitti, M. Shape-programmable magnetic soft matter. *Proc. Natl. Acad. Sci. U.S.A.* **2016**, *113*, E6007–E6015.
- (47) Ze, Q.; Kuang, X.; Wu, S.; Wong, J.; Montgomery, S. M.; Zhang, R.; Kovitz, J. M.; Yang, F.; Qi, H. J.; Zhao, R. Magnetic shape memory polymers with integrated multifunctional shape manipulation. *Adv. Mater.* **2020**, *32*, No. 1906657.
- (48) Ma, C.; Wu, S.; Ze, Q.; Kuang, X.; Zhang, R.; Qi, H. J.; Zhao, R. Magnetic Multimaterial Printing for Multimodal Shape Transformation with Tunable Properties and Shiftable Mechanical Behaviors. ACS Appl. Mater. Interfaces 2020, No. 13863.
- (49) Zhao, Q.; Zou, W.; Luo, Y.; Xie, T. Shape memory polymer network with thermally distinct elasticity and plasticity. *Sci. Adv.* **2016**, 2, No. e1501297.
- (50) Davidson, E. C.; Kotikian, A.; Li, S.; Aizenberg, J.; Lewis, J. A. 3D Printable and Reconfigurable Liquid Crystal Elastomers with Light-Induced Shape Memory via Dynamic Bond Exchange. *Adv. Mater.* **2020**, 32, No. e1905682.
- (51) Jiang, Z. C.; Xiao, Y. Y.; Zhao, Y. Shining Light on Liquid Crystal Polymer Networks: Preparing, Reconfiguring, and Driving Soft Actuators. Advanced. *Adv. Opt. Mater.* **2019**, *7*, No. 1900262.
- (52) Lv, C.; Xia, H.; Shi, Q.; Wang, G.; Wang, Y.-S.; Chen, Q.-D.; Zhang, Y.-L.; Liu, L.-Q.; Sun, H.-B. Sensitively Humidity-Driven Actuator Based on Photopolymerizable PEG-DA Films. *Adv. Mater. Interfaces* **2017**, *4*, No. 1601002.
- (53) Palleau, E.; Morales, D.; Dickey, M. D.; Velev, O. D. Reversible patterning and actuation of hydrogels by electrically assisted ionoprinting. *Nat. Commun.* **2013**, *4*, No. 2257.
- (54) Traugutt, N. A.; Mistry, D.; Luo, C.; Yu, K.; Ge, Q.; Yakacki, C. M. Liquid-Crystal-Elastomer-Based Dissipative Structures by Digital Light Processing 3D Printing. *Adv. Mater.* **2020**, *32*, No. e2000797.
- (55) He, Q.; Wang, Z.; Wang, Y.; Minori, A.; Tolley, M. T.; Cai, S. Electrically controlled liquid crystal elastomer-based soft tubular actuator with multimodal actuation. *Sci. Adv.* **2019**, *5*, No. eaax5746.
- (56) Guin, T.; Settle, M. J.; Kowalski, B. A.; Auguste, A. D.; Beblo, R. V.; Reich, G. W.; White, T. J. Layered liquid crystal elastomer actuators. *Nat. Commun.* **2018**, *9*, No. 2531.
- (57) Kotikian, A.; Truby, R. L.; Boley, J. W.; White, T. J.; Lewis, J. A. 3D Printing of Liquid Crystal Elastomeric Actuators with Spatially Programed Nematic Order. *Adv. Mater.* **2018**, *30*, No. 1706164.
- (58) Ware, T. H.; McConney, M. E.; Wie, J. J.; Tondiglia, V. P.; White, T. J. Voxelated liquid crystal elastomers. *Science* **2015**, 347, 982–984.
- (59) Saed, M. O.; Torbati, A. H.; Nair, D. P.; Yakacki, C. M. Synthesis of Programmable Main-chain Liquid-crystalline Elastomers Using a Two-stage Thiol-acrylate Reaction. *J. Visualized Exp.* **2016**, No. e53546.

- (60) Saed, M. O.; Volpe, R. H.; Traugutt, N. A.; Visvanathan, R.; Clark, N. A.; Yakacki, C. M. High strain actuation liquid crystal elastomers via modulation of mesophase structure. *Soft Matter* **2017**, 13, 7537–7547.
- (61) Pei, Z.; Yang, Y.; Chen, Q.; Terentjev, E. M.; Wei, Y.; Ji, Y. Mouldable liquid-crystalline elastomer actuators with exchangeable covalent bonds. *Nat. Mater.* **2014**, *13*, 36–41.
- (62) Zhang, Y.; Wang, Z.; Yang, Y.; Chen, Q.; Qian, X.; Wu, Y.; Liang, H.; Xu, Y.; Wei, Y.; Ji, Y. Seamless multimaterial 3D liquid-crystalline elastomer actuators for next-generation entirely soft robots. *Sci. Adv.* **2020**, *6*, No. eaay8606.
- (63) Liu, X.; Kim, S.-K.; Wang, X. Thermomechanical liquid crystalline elastomer capillaries with biomimetic peristaltic crawling function. *J. Mater. Chem. B* **2016**, *4*, 7293–7302.
- (64) Yang, Y.; Zhan, W.; Peng, R.; He, C.; Pang, X.; Shi, D.; Jiang, T.; Lin, Z. Graphene-Enabled Superior and Tunable Photomechanical Actuation in Liquid Crystalline Elastomer Nanocomposites. *Adv. Mater.* **2015**, *27*, 6376–81.
- (65) Ahn, S.-k.; Ware, T.; Lee, K.; Tondiglia, V.; White, T. Shape Programmable Materials from Photoresponsive Liquid Crystalline Elastomers. In *Abstracts of Papers of the American Chemical Society*; American Chemical Society: 1155 16th Street, NW, Washington, DC, 2015; Vol. 250, pp 433.
- (66) Ohm, C.; Brehmer, M.; Zentel, R. Liquid crystalline elastomers as actuators and sensors. *Adv. Mater.* **2010**, *22*, 3366–3387.
- (67) Yakacki, C.; Saed, M.; Nair, D.; Gong, T.; Reed, S.; Bowman, C. Tailorable and programmable liquid-crystalline elastomers using a two-stage thiol—acrylate reaction. *RSC Adv.* **2015**, *5*, 18997—19001.
- (68) Saed, M. O.; Torbati, A. H.; Nair, D. P.; Yakacki, C. M. Synthesis of programmable main-chain liquid-crystalline elastomers using a two-stage thiol-acrylate reaction. *J. Visualized Exp.* **2016**, *107*, No. e53546.
- (69) Liu, Y.; Wang, X. J.; Xu, Y. M.; Xue, Z. G.; Zhang, Y.; Ning, X.; Chen, X.; Xue, Y. G.; Lu, D.; Zhang, Q. H.; Zhang, F.; Liu, J. X.; Guo, X. G.; Hwang, K. C.; Huang, Y. G.; Rogers, J. A.; Zhang, Y. H. Harnessing the interface mechanics of hard films and soft substrates for 3D assembly by controlled buckling. *Proc. Natl. Acad. Sci. U.S.A.* **2019**, *116*, 15368–15377.
- (70) Xu, S.; Yan, Z.; Jang, K. I.; Huang, W.; Fu, H. R.; Kim, J.; Wei, Z.; Flavin, M.; McCracken, J.; Wang, R.; Badea, A.; Liu, Y.; Xiao, D. Q.; Zhou, G. Y.; Lee, J.; Chung, H. U.; Cheng, H. Y.; Ren, W.; Banks, A.; Li, X. L.; Paik, U.; Nuzzo, R. G.; Huang, Y. G.; Zhang, Y. H.; Rogers, J. A. Assembly of micro/nanomaterials into complex, three-dimensional architectures by compressive buckling. *Science* **2015**, *347*, 154–159.
- (71) Kim, Y.; Yuk, H.; Zhao, R.; Chester, S. A.; Zhao, X. Printing ferromagnetic domains for untethered fast-transforming soft materials. *Nature* **2018**, *558*, 274–279.
- (72) Harada, M.; Ando, J.; Hattori, S.; Sakurai, S.; Sakamoto, N.; Yamasaki, T.; Masunaga, H.; Ochi, M. In-situ analysis of the structural formation process of liquid—crystalline epoxy thermosets by simultaneous SAXS/WAXS measurements using synchrotron radiation. *Polym. J.* **2013**, *45*, 43–49.
- (73) Tammer, M.; Li, J.; Komp, A.; Finkelmann, H.; Kremer, F. FTIR-Spectroscopy on Segmental Reorientation of a Nematic Elastomer under External Mechanical Fields. *Macromol. Chem. Phys.* **2005**, *206*, 709–714.
- (74) Coates, J. Interpretation of Infrared Spectra A Practical Approach. In *Encyclopedia of Analytical Chemistry: Applications, Theory and Instrumentation*; Wiley, 2000; Vol. 12, pp 10815–10837.
- (75) Hanzon, D. W.; Traugutt, N. A.; McBride, M. K.; Bowman, C. N.; Yakacki, C. M.; Yu, K. Adaptable liquid crystal elastomers with transesterification-based bond exchange reactions. *Soft Matter* **2018**, *14*, 951–960.